The Journal of Experimental Biology 204, 1817–1830 (2001)
Printed in Great Britain © The Company of Biologists Limited 2001
JEB3533



# THE DYNAMICS AND SCALING OF FORCE PRODUCTION DURING THE TAIL-FLIP ESCAPE RESPONSE OF THE CALIFORNIA SPINY LOBSTER *PANULIRUS INTERRUPTUS*

JENNIFER C. NAUEN* AND ROBERT E. SHADWICK

*Scripps Institution of Oceanography, University of California at San Diego, La Jolla, CA 92093-0204, USA*

*Present address: Department of Organismic and Evolutionary Biology, Harvard University, 26 Oxford Street, Cambridge, MA 02138, USA (e-mail: jnauen@oeb.harvard.edu)

*Accepted 3 February; published on WWW 23 April 2001*

## Summary

**The tail-flip escape behavior is a stereotypical motor pattern of decapod crustaceans in which swift adduction of the tail to the thorax causes the animal to rotate, move vertically into the water column and accelerate rapidly backwards. Previous predictions that a strong jet force is produced during the flip as the tail adducts to the body are not supported by our simultaneous measurements of force production (using a transducer) and the kinematics (using high-speed video) of tail-flipping by the California spiny lobster *Panulirus interruptus*. Maximum force production occurred when the tail was positioned approximately normal to the body. Resultant force values dropped to approximately 15 % of maximum during the last third of the flip and continued to decline as the tail closed against the body. In addition, maximum acceleration of the body of free-swimming animals occurs when the tail is positioned approximately normal to the body, and acceleration declines steadily to negative values as the tail continues to close. Thus, the tail appears to act largely as a paddle. Full flexion of the tail to the body probably increases the gliding distance by reducing drag and possibly by enhancing fluid circulation around the body.**

**Morphological measurements indicate that *Panulirus interruptus* grows isometrically. However, measurements of tail-flip force production for individuals with a body mass ($M_b$) ranging from 69 to 412 g indicate that translational force scales as $M_b^{0.83}$. This result suggests that force production scales at a rate greater than that predicted by the isometric scaling of muscle cross-sectional area ($M_b^{2/3}$), which supports previously published data showing that the maximum accelerations of the tail and body of free-swimming animals are size-independent. Torque ($\tau$) scaled as $M_b^{1.29}$, which is similar to the hypothesized scaling relationship of $M_b^{4/3}$. Given that $\tau \propto M_b^{1.29}$, one would predict rotational acceleration of the body ($\alpha$) to decrease with increasing size as $M_b^{-0.37}$, which agrees with previously published kinematic data showing a decrease in $\alpha$ with increased $M_b$.**

Key words: caridoid, escape response, tail-flip, acceleration, crustacean, swimming, locomotion, force transducer, California spiny lobster, *Panulirus interruptus*.

## Introduction

The tail-flip escape behavior is a stereotyped motor act that is a key feature of eumalocostracans (Heitler et al., 2000). During the flip, the tail is swiftly adducted to the body and the animal is accelerated upwards and backwards. As the center of mass ($C_m$) of the animal is anterior to the site of force production, a moment is also produced during the tail-flip that rotates the animal.

The kinematics of tail-flips by lobster (Newland et al., 1988; Cromarty et al., 1991; Spanier et al., 1991; Nauen and Shadwick, 1999), crayfish (Webb, 1979), shrimp (Daniel and Meyhöfer, 1989; Arnott et al., 1998) and stomatopods (Heitler et al., 2000) has been studied, but the hydrodynamic force balance of this escape response is not well understood. Added mass dominates the tail-flip because the motion is unsteady. In addition, it has been proposed that, as the tail closes against the body and the fluid between these two surfaces is displaced, a strong and directed jet of water is formed that contributes to thrust production. Daniel and Meyhöfer (Daniel and Meyhöfer, 1989) dubbed this source of thrust the ‘squeeze force’ and included calculations of the squeeze force in their mathematical model of tail-flip force production for the caridean shrimp *Pandalus danae*.

The computational model of tail-flip mechanics of Daniel and Meyhöfer (Daniel and Meyhöfer, 1989) indicated that the squeeze force contributes a substantial amount of the total force of the flip and much of the force in the latter third of the flip as the tail closes against the body. Thus, they concluded that ‘during the last stages of the tail-flip, nearly all the thrust

produced arises from the squeeze force' (Daniel and Meyhöfer, 1989) and that neglect of this force would lead to underestimates of total force production and, thus, underestimates of animal performance. One goal of the present study was to determine empirically the contribution of the squeeze force to thrust production by making the first measurements of force production during the tail-flip and correlating these measurements with the kinematics of the tail.

Quantifying force production and kinematics in a size range of animals also allowed us to test two hypotheses about the scaling of tail-flip force production. The fact that force output from a muscle fiber is proportional to its cross-sectional area is the basis of the hypothesis that, given isometric growth, muscle force will scale as body mass ($M_b$) to the power 2/3. Daniel and Meyhöfer (Daniel and Meyhöfer, 1989) used that relationship to predict that maximum acceleration of the body (a key variable for this escape response) will scale as $M_b^{-1/3}$ (i.e. $M_b^{2/3}/M_b^1$, given force = mass × acceleration). Previous measurements of free-swimming *Panulirus interruptus* indicated that maximum acceleration of the body was independent of body size (Nauen and Shadwick, 1999), as has been documented for tail-flips by brown shrimp *Crangon crangon* (Arnott et al., 1998) and fast-starts by fish (Webb, 1976; Domenici and Blake, 1993). Such a finding suggests that muscle force output scales with a mass exponent greater than 2/3. To test this hypothesis on *P. interruptus*, we measured the translational forces produced by a size range of animals. We also measured the torque ($\tau$) produced during the tail-flip to test the prediction that $\tau$ will scale as $M_b^{4/3}$, given that the hydrodynamic forces dependent on acceleration (added-mass and squeeze forces) scale to body volume, or $M_b^1$, and that lever arm scales as $M_b^{1/3}$ for isometric growth (Daniel and Meyhöfer, 1989).

The spiny lobster *Panulirus interruptus* is a good model system for the tail-flip escape response because post-larval individuals increase in body mass by more than four orders of magnitude through isometric growth, and animals of all sizes retain the ability to tail-flip (Nauen and Shadwick, 1999). We measured the vertical forces, horizontal forces and torque produced during tail-flipping by individuals with a body mass of 69–412 g attached to a force transducer, and correlated the dynamics of force production with simultaneously collected high-speed video images to test the jet force hypothesis. Comparison of the present tail kinematic data with previously published values from free-swimming individuals of *P. interruptus* (Nauen and Shadwick, 1999) allowed us to test for the effects of attachment to the force transducer on tail-flip performance.

## Materials and methods

*Panulirus interruptus* (Randall) were collected from local coastal waters using SCUBA. They were housed in flow-through seawater tanks at ambient temperature and had open access to their native diet of mussels and sea urchins (Tegner and Levin, 1983). Growth is isometric in *Panulirus interruptus*, so little sexual dimorphism is seen in the characteristics that contribute to swimming performance (Nauen and Shadwick, 1999) and both males and females were used for force measurements. Selection of the intermolt animals used was based solely on body size (Table 1).

Multiple individuals of very similar size were not available. However, in a previous study of *Panulirus interruptus* (Nauen and Shadwick, 1999), we determined that, for variables including the speed and acceleration of the tail, the distance traveled, maximum speed and maximum acceleration of the center of mass ($C_m$) of the body, and the maximum rotation, rotational velocity and rotational acceleration of the body, the variation among individuals of similar size was not statistically different from the variation associated with multiple events from a single individual of that size. In other words, mean values of variables based on repeated flip events by individuals of a given body mass were representative of data for multiple individuals of that body mass. On the basis of this result, the present scaling data are mean values from five tail-flip events by single animals of different sizes.

### *Force measurements*

The animals were tested using a force plate based on the design of Full and Tu (Full and Tu, 1990), but modified for use with an aquatic animal and for direct measurement of torque (Fig. 1). The force transducer consisted of hollow brass box-beams (1.9 cm in cross section) and a hollow brass cylinder (0.64 cm in diameter) in series with an attachment site for the animal. Double cantilevers were made in the transducer by machining rectangular openings in the sides of the box-beams.

Table 1. *Kinematics and force measurements for* Panulirus interruptus

| Body mass (g) | Body length (mm) | Sex | Tail $S_{Max}$ ($m\,s^{-1}$) | Tail $A_{Max}$ ($m\,s^{-2}$) | Flip duration (ms) | $F_{VMax}$ (N) | $F_{HMax}$ (N) | $\tau_{Max}$ (N m) | $F_{RMax}$ (N) | θ at $F_{RMax}$ (degrees) | β at flip initiation (degrees) | β at $F_{VMax}$ (degrees) | β at $F_{HMax}$ (degrees) |
|---|---|---|---|---|---|---|---|---|---|---|---|---|---|
| 69 | 138 | F | 1.7±0.2 | 37±14 | 87±15 | 3.7±1.0 | 5.2±0.4 | 0.15±0.03 | 5.2±0.5 | −2±8 | 155±27 | 125±20 | 84±7 |
| 115 | 160 | F | 1.3±0.3 | 38±10 | 92±13 | 2.1±0.9 | 4.2±1.6 | 0.14±0.04 | 4.4±1.6 | 15±9 | 145±31 | 99±18 | 75±9 |
| 165 | 180 | M | 1.7±0.2 | 35±12 | 122±11 | 2.8±0.5 | 6.8±1.3 | 0.38±0.10 | 8.1±0.5 | 14±3 | 148±13 | 114±15 | 88±13 |
| 281 | 220 | M | 1.5±0.1 | 41±10 | 109±10 | 3.7±0.9 | 12.7±0.4 | 0.73±0.09 | 12.7±0.5 | −3±3 | 83±6 | 80±7 | 67±10 |
| 412 | 245 | M | 2.0±0.2 | 48±9 | 129±14 | 8.8±0.5 | 19.1±5.6 | 1.23±0.45 | 19.8±6.1 | 9±10 | 112±18 | 98±10 | 75±13 |

*S*, speed; *A*, acceleration; Max, maximum value; *F*, force; V, vertical; H, horizontal; τ, torque; R, resultant; θ, trajectory angle; β, tail angle. Values are means ± S.D. for five flips per individual.

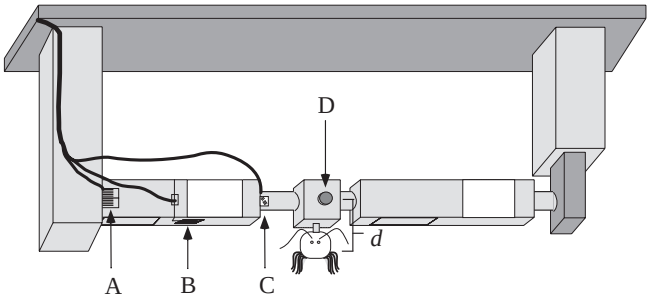


Fig. 1. Schematic diagram of the force transducer (not to scale) with gauges for measuring fore–aft or horizontal forces (A), vertical forces (B) and torque (C). The animal was attached to the transducer *via* a bolt cemented to its cephalothorax (detailed in Fig. 3); the bolt slid into the block and was fixed in place by a set screw (D). The set screw is positioned at the neutral axis of the transducer, which is distance (*d*) above the center of mass of the animal (shown in Fig. 3).

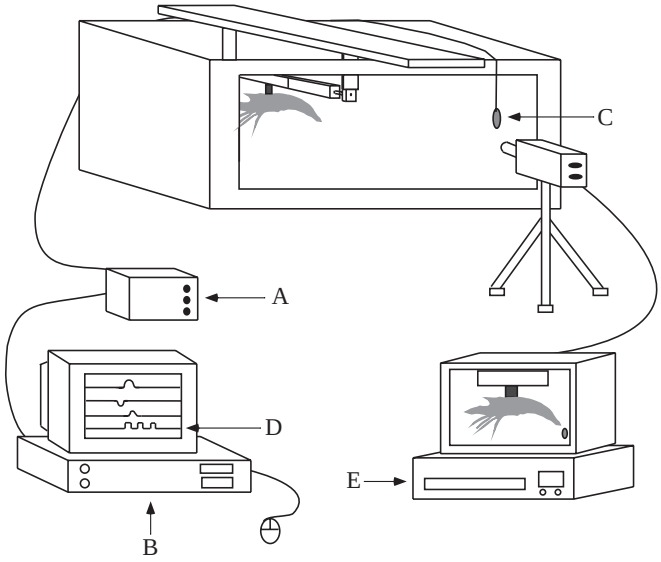


Fig. 2. Apparatus used to record force production during the tail-flip escape response of the lobster. Data from the force transducer were amplified (A) before being digitally recorded (B) on a PC-type computer. Activation of a light-emitting diode (LED) (C) in view of the camera was recorded as a change in voltage on the fourth channel of the data-collection program (D) to synchronize the force and kinematic events. Video images of a lateral view of the animal and the LED were simultaneously recorded on a video recorder at 180 frames $s^{-1}$ (E).

Strain gauges (120 Ω except for the 360 Ω torsional gauges; Omega) were bonded to the outer surfaces of the cantilevers and the cylinder. The stiffness of the system was increased by bonding brass beams 4 mm in height to one side of the fore–aft and vertical cantilevers to increase the resonant frequency of the transducer. Mechanical cross-talk between the gauges was minimized by welding a small piece of telescoping box-beam to the section of the beam between the cantilevers to further isolate each sensitive element.

The resonant frequencies of the unloaded torsional, vertical and fore–aft gauges were 320, 200 and 170 Hz, respectively. The effect of the load of the animals on the response of the transducer was assessed by measuring the exponential decay of the amplitude of a free vibration of the transducer with loads of 69–414 g. The time constant of the decay is the damping constant. The damping constant relative to the resonant frequency, or the damping ratio of the force transducer, ranged from 0.02 to 0.05, which is very low. We used the worst-case scenario of 0.05, and calculated the amplitude and phase shift of the signal as a function of the driving frequency and load (0, 69 or 414 g) using the equations for a simple oscillating system (Milnor, 1982). The calculations indicated that, at the primary frequencies of the force signals, signal output from the transducer was amplified by less than 2 % and phase-shifted by less than 0.1 ms. Note that the phase shift was much less than the 5.5 ms temporal resolution of the video images. Thus, because of the degree of damping in this system, the effects of the mass of the animal on the characteristics of signal output from the transducer were negligible.

Gauges were calibrated using five static loads from 4.5 to 29.4 N before and after each experiment. Torsional gauges were calibrated using the same static loads applied over a lever arm of known distance. The transducer showed a linear response to loads in this range.

The fore–aft and vertical gauges were wired in a full Wheatstone bridge arrangement; the torsional gauge was wired in a half Wheatstone bridge arrangement. Direct current output from the strain gauges was amplified using CyberAmps (Axon Instruments) and collected at a rate of 1000 Hz on an IBM PC-type computer using Axotape (Axon Instruments). The transducer was firmly attached to brass blocks fixed to an aluminum plate; the plate was bolted to the wooden frame of a 170 l aquarium (Fig. 2). Exposed wiring was coated with epoxy resin for waterproofing, and the transducer was submerged in sea water. The water temperature was 19±1 °C during the experiments.

A bolt and an aluminum plate were bonded dorsally to the cephalothorax of each animal (Fig. 3) using Splash Zone

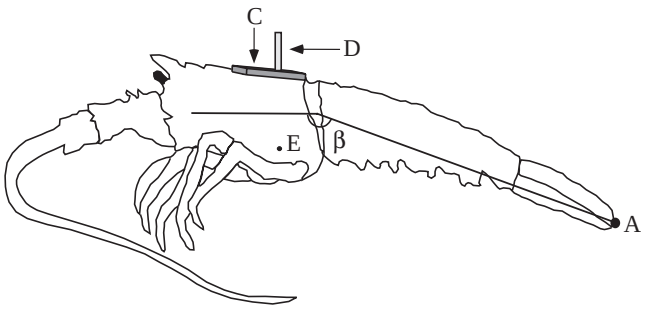


Fig. 3. Diagram of *Panulirus interruptus* showing the points digitized, the method of attachment of the force transducer, the digitized point at the tip of the tail (A), and determination of the angle between the tail and the body (β). In this case, β=160 °. The plate (C) provided increased surface area for bonding the bolt (D) to the animal for attachment to the transducer. The bolt was placed over the center of mass (E; Nauen and Shadwick, 1999).

cement (Koppers) because it cures under water and provides strong bonds that last of the order of weeks. The plate provided an increased surface area for attachment to the animal; the bolt inserted into a block on the transducer (Fig. 1) and was positioned dorsally above the $C_m$ of the animal (the position of the $C_m$ is relatively stable during a tail-flip; Nauen and Shadwick, 1999).

The tail-flip is a stereotyped motor act mediated by giant fiber nerves (Wine, 1984). Tail-flip characteristics, including the direction and height of the flip and the number of flips in a swimming sequence, are dependent on the type of stimulus, its application point on the body and whether the animal is in an intermolt or intramolt period (Cromarty et al., 1991). Stimulation to the anterior region of the cephalothorax results in a flip trajectory that is essentially straight backwards (Newland et al., 1992). When attached to the transducer, the animals responded most consistently to a fast tap of the antennae by hand. This stimulus repeatedly elicited the tail-flip response, and no side effects from the stimulus were observed. To mimic standing on a substratum, we provided a small platform for the animals; however, in the presence of a platform, a series of animals did not respond to a variety of stimuli. As a result, the data were collected without a platform beneath the legs of the animals.

The first five flips in which the tail closed symmetrically (without transverse rotation) were analyzed for each animal. The voltage data were imported into Acqknowledge software (BIOPAC Systems) and transformed using the calibration relationships.

Two types of noise were present in the force data: (i) occasional 60 Hz noise, and (ii) high-frequency noise (greater than 100 Hz) produced by the animal both during and between flips. The high-frequency noise was not correlated with the position of the tail, legs or antennae of the animal with respect to the transducer. It was correlated with a relatively high-frequency rasping sound produced by the lobsters by rubbing the base of their antennae against the cephalothorax. Frequency analysis using Acqknowledge software (BIOPAC Systems) indicated that the noise was composed primarily of high-frequency components (100–240 Hz) and that the primary components of the force data were between 10 and 20 Hz. Thus, to remove this noise, all the force data were filtered with a 55 Hz Blackman low-pass filter with 250 coefficients (to ensure a sharp filtering cut-off) in Acqknowledge software. The use of this filtering method on force data that did not contain high-frequency noise indicated that signal amplitude was diminished by less than 3 % and that phase shifts were not introduced into the data.

The resultant translational force ($F_R$) and its vector angle ($\theta$) were calculated from the horizontal ($F_H$) and vertical ($F_V$) forces as follows:

$$F_R = (F_H^2 + F_V^2)^{0.5}, \quad (1)$$

$$\theta = \arctan(F_V/F_H). \quad (2)$$

$F_R$ and $\theta$ represent the magnitude and trajectory, respectively, of the resultant translational force acting on the $C_m$. This force is distinct from the torque ($\tau$; i.e. the rotational force) that exists because thrust is produced at some distance from the $C_m$.

Torque is produced during the tail-flip because the abdominal muscle that powers the flip is posterior to the $C_m$ of the animal; the force produced by that muscle acts over the distance between the muscle and the $C_m$ to produce torque. We called this torque $\tau_l$ because it is produced by the animal. The torsional gauges were also deflected by an artificial torque produced as a result of the structure of the transducer. The artifact was produced because the animal's $C_m$ was located at some distance ($d$) below the neutral axis of the transducer (Fig. 1). Therefore, the forces acting on the $C_m$ of the animal acted on the transducer over a distance $d$, which produced torque that was an artifact of transducer design ($\tau_a$). The magnitude of $\tau_a$ was estimated by multiplying the amplitude of the horizontal force by $d$. Subtracting $\tau_a$ from the torsional signal gave $\tau_l$. The amplitude of $\tau_a$ was typically similar in magnitude to that of $\tau_l$. For simplicity, $\tau_l$ is referred to as $\tau$ for the remainder of the paper.

The maximum amplitude was determined for each force trace. The duration of the flip was determined from the video images because small high-frequency movements of the tail at flip initiation (such as fanning out the uropods) caused very small but frequent deviations from baseline on the force traces. The timing of $F_H$, $F_R$ and $\tau$ was determined relative to the time of maximum $F_V$ ($F_{VMax}$), which was typically a reliable first event in the force recordings.

### *Kinematics*

Video images of a lateral view of the tethered animals were collected simultaneously with the force measurements using a Peak Performance high-speed video system with an HSC-180 NM camera and a Panasonic AG-5700 video recorder recording at 180 fields $s^{-1}$ (Fig. 2). The video images were synchronized with the force traces using a light-emitting diode (LED) that flashed in view of the camera. The voltage of the LED was recorded with the force traces so that, when the LED was manually activated, a light pulse was recorded in the corner of the video image and a square wave was recorded on one channel of the force traces (Fig. 2). The video speed was selected to ensure that approximately 15–30 images were collected for each tail-flip event.

Video images were imported into a Macintosh Quadra 700 using a Panasonic AG-7355 video recorder and MediaGrabber 2.2 software (RasterOps Corp.). Images were digitized using the public-domain NIH Image program (developed at the US National Institutes of Health and available at http://rsb.info.nih.gov/nih-image/). The position of the tip of the tail and a fixed reference point on the image were digitized. The reference points were used to ensure that the position of the video field in the analysis program was consistent.

The speed and acceleration of the tail were calculated using the digitized position data. This type of calculation can be subject to large error because of high-frequency noise that is inherent in digitized position data from sources including

camera vibrations and digitizing errors (Biewener and Full, 1992). To overcome this problem, the position data were imported into Acqknowledge software, and a zero-lag low-pass Blackman digital filter with 250 coefficients was applied. The critical filtering frequencies used on the kinematic data were different from those used on the force data because the tips of the tails often showed small high-frequency movements at the initiation and end of the tail-flip. The critical filter frequency for each kinematic data set was determined by considering the duration of each event to represent the period of its fundamental frequency ($f_o$). The filter frequency for each data set was $3.33f_o$. Speed was calculated as:

$$S_t = (x_{t+i} - x_{t-i})/(2\Delta t)\,, \quad (3)$$

where $S$ is speed, $t$ is time, and $x_{t+i}$ or $x_{t-i}$ is the position at time $t+i$ or time $t-i$, respectively (Winter, 1989). Acceleration was calculated by substituting $S$ for $x$ in equation 3. This equation effectively filters the data because each calculated value is dependent on non-adjacent video frames, but it does not decrease the temporal resolution of the data. The use of the Winter equation allows us to compare the present kinematic data with previously published values from free-swimming animals calculated using the same method (Nauen and Shadwick, 1999).

To describe the position of the tail relative to the body at points of interest during the flips, the image data were synchronized with the force trace using the LED and square-wave markers (Fig. 2). The angle of the tail relative to the body (β) was determined by drawing a straight line through the anterior–posterior axis of the body and a second line parallel to the long axis of the tail (Fig. 3). Using this method, β was 180 ° if the tail extended out completely straight from the body and approximately 15 ° (not 0 °) when the tail was closed against the body. Note that the abdomen is segmented and jointed so that, as the tail closes, the vertex of β shifts posteriorly. Tail angle data were not filtered.

### *Testing for methodological effects*

To test for the effects of tethering on tail-flip kinematics, we compared values of velocity and acceleration of the tip of the tail for tethered animals (five animals, five events per animal, 69–412 g $M_b$) with previously published data for free-swimming animals of a very similar range of body mass (three animals, four events per animal, 59–432 g $M_b$; Nauen and Shadwick, 1999). In brief, the previous study examined the tail-flip kinematics of free-swimming *Panulirus interruptus*. Tail-flips were elicited using an electrical stimulus, and tail-tip velocity and acceleration were calculated from video images using the methods described here (for more details of the experiments with free-swimming animals, see Nauen and Shadwick, 1999).

The data available on the kinematics of free-swimming animals also allowed us to test for the effects of size on the timing of tail-flip kinematics and the potential production of a jet force. The resonant frequency of the force transducer limited the body mass of animals tested in this study to a range of approximately 70–400 g. However, results from the force data can be compared with kinematic data for free-swimming individuals of *Panulirus interruptus* ranging in $M_b$ from 1 to 1000 g (Nauen and Shadwick, 1999). To test for the effects of size on the timing of force production, images of free-swimming animals were synchronized with calculations of the distance, speed and acceleration of the $C_m$ (using the methods described here) to determine β at the times of maximum body speed and acceleration.

### *Statistical analyses*

Statistical analyses were conducted using STATGRAPHICS software (Manguistics). Statistical significance was established using a probability value of 0.05. $F$ values for analyses of variance (ANOVAs) were calculated as described by Zar (Zar, 1984). One-way analyses of variance were used to determine whether the values of β for individual animals differed at specific points of interest in the flip (such as flip initiation, maximum $F_H$ and maximum $F_V$), and whether the trajectory angle (θ) of different individuals varied at maximum $F_R$ ($F_{RMax}$). To determine the effect of individual and position of the tail (β) on the values of $F_{RMax}$, a two-factor ANOVA was performed in which individual was the random effect and tail angle was the fixed effect. A nested ANOVA was used to compare the tail kinematic data of tethered and free-swimming animals because different individuals were used for each set of experiments (Zar, 1984). A two-factor fixed ANOVA was used to compare the values of β for free-swimming animals at the times of maximum body speed and acceleration.

Force and kinematic data were analyzed with respect to animal size (represented by $M_b$) for scaling analyses. Regression relationships were fitted to mean values of the variable for each individual because single individuals of each size were measured, as discussed above. Slopes calculated with mean values were not significantly different (and were identical in seven out of the eight cases) from slopes calculated using the raw data and the 'computation of regression with more than one $Y$ per value of $X$' method (Sokal and Rohlf, 1995). Given this similarity in results, we fitted the regression models to mean values of the data to compare the present results with previously published regression relationships for free-swimming animals calculated using that method (Nauen and Shadwick, 1999).

The exponential relationship $y=aM_b^c$ was applied to the data, where the slope ($c$) and $y$ intercept ($a$, at $M_b$=1) of the relationship determine the scaling equation. The data were log-transformed and fitted with a linear regression model ($\log_{10}y=\log_{10}a+c\log_{10}M_b$) (as proposed by Huxley, 1932). The ordinary least-squares (OLS) regression model assumes (incorrectly in this case) that the values of $M_b$ are determined without error. This assumption is not made for reduced-major-axis (RMA) regression models; therefore, we also calculated RMA slopes (RMA slope=OLS slope/correlation coefficient; the standard error of the RMA calculation is numerically equal to the standard error of the OLS calculation; LaBarbera, 1989). For ease of viewing, the data presented in graphical form are

plotted untransformed on logarithmic scales with statistically significant relationships indicated by power regression models. Statistically significant regression models were tested against hypothesized values using a *t*-test (as described by Zar, 1984).

## Results

### *Tail kinematics*

The pereopods (walking legs) of the tethered animals were often extended prior to flip initiation, and were adducted as the tail passed through an angle of 90 ° to the body.

Mean values of maximal tail-tip speeds varied from 1.3±0.3 to 2.0±0.2 m s$^{-1}$ among the animals (mean ± S.D., $N$=5, Fig. 4A); mean values of maximal tail-tip accelerations varied from 35±12 to 48±9 m s$^{-2}$ (mean ± S.D., $N$=5, Fig. 4B). The slopes of the regression models fitted to the tail speed and acceleration data were not significantly different from zero (*t*-test, $P$=0.45 for tail speed, $P$=0.09 for acceleration). Nested ANOVA comparisons of the maximum tail-tip speeds of the tethered animals studied here with previously published data (Nauen and Shadwick, 1999) for free-swimming animals of a similar body mass (69–412 g for tethered animals and 59–432 g for free-swimming animals) indicated a significant effect of individual on tail-tip velocity ($F$=7.5, $P$<0.05, Table 2) and tail-tip acceleration ($F$=10.4, $P$<0.05, Table 2), but no significant effect of tethering on tail-tip velocity (ANOVA, $F$=2.9, $P$>0.14, Table 2) or acceleration ($F$=5.0, $P$>0.06, Table 2).

Table 2. *Results (*F*-values) of the nested ANOVA on tail velocity and acceleration values for tethered and free-swimming animals*

| Variable | Individual | Tethering |
|---|---|---|
| d.f. | 6, 29 | 1, 6 |
| Tail-tip velocity | 7.5* | 2.9 |
| Tail-tip acceleration | 10.4* | 5 |

d.f., degrees of freedom.
*Statistically significant effect ($P$<0.05).

Tail-flip duration varied from 87±15 to 129±14 ms (mean ± S.D., $N$=5, Fig. 4C) and tended to increase with increasing body mass, although the slope of the regression model fitted to the data was not significantly different from zero (*t*-test, $P$=0.06).

At flip initiation, mean values of β for the individuals ranged from 83±6 to 155±27 ° (mean ± S.D., $N$=5, Table 1) and were significantly different among individuals (ANOVA, $F$=10.75, $P$<0.001). A Newman–Keuls *post-hoc* test indicated that values of β for the two larger animals, which tended to initiate flips with partially abducted tails (β=83±6 ° and 112±18 ° for the 281 g and 412 g animals, respectively, means ± S.D., $N$=5), were significantly different from each other and from those of the three smaller animals.

### *The timing and magnitude of force production*

In general, each of the force traces showed a single, well-defined peak. Ventral movements of the tail at flip initiation produced $F_V$ (Fig. 5), which would lift the animal. Maximum values of $F_V$ ($F_{VMax}$) were always recorded when β was greater than 70 ° (mean values ranged from 80±7 to 125±20 °, means ± S.D., $N$=5, Table 1). β values at $F_{VMax}$ were significantly different among individuals (ANOVA, $F$=6.52, $P$<0.002). During approximately half the observed flips, there was a small vertical force component recorded as negative in sign while the uropods moved upwards to close against the body (Fig. 5). The negative sign was a factor in the calculations of the $C_m$ trajectory angle, but it was not a factor in the calculation of $F_R$ because only the magnitudes of $F_H$ and $F_V$ were considered in equation 1.

Maximum values of $F_H$ ($F_{HMax}$), which would translate the animal, occurred after $F_{VMax}$ and were always recorded when β was greater than 50 ° (mean values ranged from 67±10 to 88±13 °, means ± S.D., $N$=5, Table 1). β values at $F_{HMax}$ were significantly different among individuals (ANOVA, $F$=3.08, $P$<0.039). $F_{HMax}$ tended to be 2–3 times greater in magnitude than $F_{VMax}$ (Fig. 5; Table 1).

The lag times between $F_{HMax}$ and $F_{VMax}$ ranged from approximately 15 to 40 % of flip duration. In general, the rise times of $F_H$ were approximately twice as long in duration as the decays. $F_V$ showed the opposite trend: rise times were

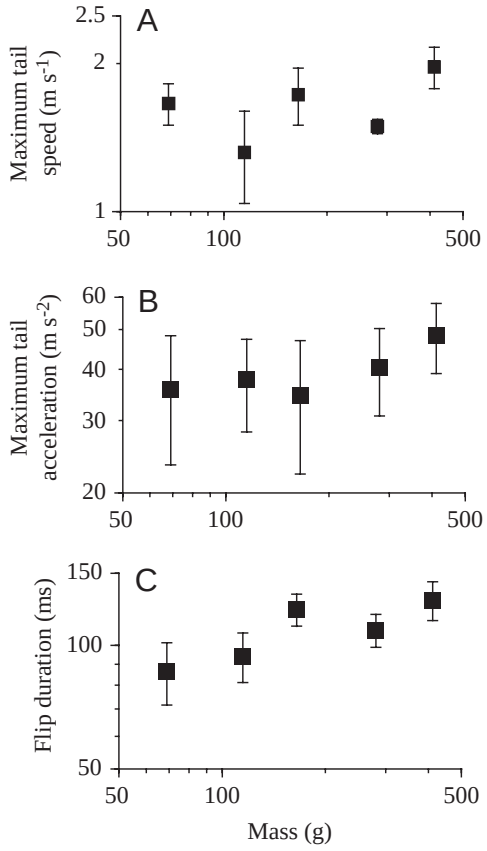


Fig. 4. The maximum speed (A) and acceleration (B) of the tip of the tail during the tail-flip and tail-flip duration (C) plotted against body mass. Values are means ± S.D. ($N$=5).

approximately half decay times. Because of these differences in rise and decay times, the approximately linear declines of $F_V$ and $F_H$ were completed at similar times despite the timing differences between the maximum values of those variables (Fig. 5).

The rise in torque ($\tau$) usually coincided with rises in $F_V$ (Fig. 5); maximum values of $\tau$ ($\tau_{Max}$) typically occurred temporally close to, but after, $F_{VMax}$ (lag times were 1–14 % of flip duration). The fall-off in $\tau$ was typically approximately linear and similar in timing to the fall-off in $F_H$ and $F_V$ (Fig. 5).

The calculated time course and magnitude of the resultant force $F_R$ were similar to those of $F_H$ (e.g. Figs 5, 6A). $F_R$ traces typically showed a single well-defined peak, which declined approximately linearly as the tail was closing and $\beta$ decreased from approximately 70 to 15 ° (Fig. 6A). Calculations of $F_R$ never showed a second force peak of appreciable magnitude during the last third of the flip.

The vector angle of $F_R$ ($\theta$) typically reached its maximum value early in the flip, when the magnitude of $F_R$ was relatively low, and declined as $F_R$ increased (Fig. 6B). For the event shown in Fig. 6, $\theta$ varied from approximately 10 to 30 ° for the duration of high resultant forces (Fig. 6C). At the time of $F_{RMax}$ (Fig. 6C), values of $\theta$ ranged from –3±3 to 15±9 ° (means ± S.D., $N$=5, Table 1) and differed significantly among individuals (ANOVA, $F$=6.99, $P$<0.011), but were independent of $M_b$ because the slope of a regression line fitted to the data was not significantly different from zero ($t$-test, $P$>0.35).

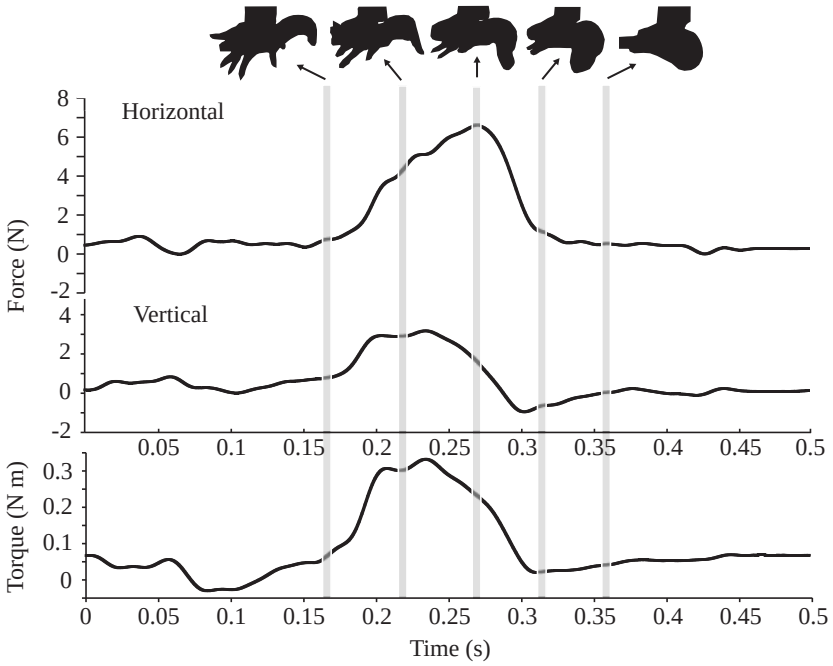


Fig. 5. Horizontal ($F_H$), vertical ($F_V$) and torsional ($\tau$) forces produced during a tail-flip by an animal of body mass 165 g. The gray boxes indicate the timing and duration (1/180 s) of the traced video images. A lateral view of the animal at that time point (traced from a video image) is shown above the graph (anterior is to the left). The vector of positive $F_H$ is to the right, positive $F_V$ is up and positive $\tau$ is counterclockwise. The calculated resultant force and trajectory for this tail-flip are shown in Fig. 6.

The timing of maximum force production varied somewhat among the animals (for example, mean values of $\beta$ at $F_{HMax}$ varied from 67 to 88 °, Table 1). However, a two-factor ANOVA of the magnitude of $F_R$ (% of $F_{RMax}$) as a function of individual and $\beta$ at the specific $\beta$ values of 90, 75, 45, 30 and 20 ° showed significant effects of $\beta$ ($P$<0.05, Table 3) but no significant effect of individual or an interaction effect of individual × $\beta$ ($P$>0.1 and 0.2, respectively, Table 3). Therefore, data from the five individuals were grouped for analysis (Fig. 7). When averaged, the peak in the resultant force occurred at tail angles of 90–75 ° (Fig. 7). The highest mean values of $F_R$ are approximately 80 % of $F_{RMax}$ (with relatively large standard deviations of approximately 20 %) because of differences among the animals in the timing of maximum force production relative to $\beta$. Regardless of these small timing differences early in the flip, when the tail was approximately normal to the body, $F_R$ values decline steadily at lower values of $\beta$ as the tail continued to close. Mean values of $F_R$ were approximately 25 % of $F_{RMax}$ when $\beta$=45 °, and

Table 3. *Results (*F*-values) of the two-factor ANOVA on resultant force values (% of maximum) as a function of individual and tail angle*

| Variable | Individual | Tail angle, $\beta$ | Individual × $\beta$ |
|---|---|---|---|
| d.f. | 4, 116 | 5, 20 | 20, 116 |
| Resultant force (% maximum) | 1.91 | 50.27* | 1.25 |

d.f., degrees of freedom.
*Statistically significant effect ($P$<0.05).

Table 4. *Results (*F*-values) of the two-factor fixed-effect ANOVA on the tail angle of free-swimming animals as a function of individual (body mass ranging from 1 to 1000 g) and kinematic event (maximum speed or acceleration of the center of mass)*

| Variable | Individual | Maximum speed or acceleration of the center of mass | Individual × speed or acceleration |
|---|---|---|---|
| d.f. | 3, 22 | 1, 20 | 3, 22 |
| Tail angle, $\beta$ | 0.31 | 53.5* | 2.73 |

d.f., degrees of freedom.
*Statistically significant effect ($P$<0.05).
The data evaluated for these results were collected as described by Nauen and Shadwick, 1999.

10 % of $F_{RMax}$ when β=20 °. Note that β was approximately 15 ° when the tail closed against the body because of the way this angle was defined (see Fig. 3 and the Materials and methods section).

To test for an effect of body size on the timing of force production, values of β for free-swimming animals at the time of maximum speed and acceleration of the $C_m$ were compared. A two-factor fixed-effect ANOVA on the effect of body size and kinematic event indicated a significant effect of kinematic event ($F$=53, $P$<0.05, Table 4) but no significant effect of body mass ($F$=0.31, $P$>0.80, Table 4) and no interaction effect of body mass × kinematic event ($F$=2.7, $P$=0.07, Table 4). Regardless of body size, maximum values of acceleration of the $C_m$ were reached when the tail was approximately normal to the body (β=83±19 °, mean ± S.D., $N$=15, Fig. 8). The acceleration of the $C_m$ of free-swimming animals declined steadily after this peak. On average, deceleration began when β was 35±18 ° (mean ± S.D., $N$=15, Fig. 8) and was concurrent with maximum values of body speed.

### *Scaling of force production*

$F_{HMax}$ and $\tau_{Max}$ increased as $M_b^{0.83}$ and $M_b^{1.29}$, respectively (OLS slope); the magnitude of $F_V$ was independent of $M_b$ (Fig. 9). The increase in $F_{Rmax}$ as $M_b^{0.82}$ (Fig. 9D) was extremely similar to that for $F_H$ ($M_b^{0.83}$, Fig. 9A; Table 5), which reflects the large contribution of $F_H$ to $F_R$ (Figs 5, 6; Table 1). The slopes calculated for $F_{HMax}$ and $F_{RMax}$ from the OLS and RMA regression models (Table 5) were not significantly different from the isometric slope of 2/3 (*t*-test, $P$>0.2 for all cases). The scaling of $\tau_{Max}$ as $M_b^{1.29}$ (OLS model) or $M_b^{1.34}$ (RMA model, Table 5) was not significantly different from the predicted relationship of $M_b^{4/3}$ (*t*-test, $P$>0.5 in both cases).

## Discussion

In summary, the measurements indicate that high levels of hydrodynamic force are produced during the early and middle stages of the tail-flip. Force declined steadily to low values during the last third of the flip as the tail closed against the body. For example, as β decreased from 45 to 20 ° while the tail closed against the body, $F_R$ values dropped to less than 15 % of maximum values. A plateau at high force levels or a secondary peak in force production during the last stages of tail closure, such as would be associated with the formation of a large and forward-directed jet that would contribute to thrust production, were not observed.

$F_{RMax}$ scaled as $M_b^{0.82}$, suggesting that force output increases faster than increases in muscle cross-sectional area (i.e. $M_b^{2/3}$, given the isometric growth of *Panulirus interruptus*). The scaling of $\tau_{Max}$ as $M_b^{1.29}$ suggests that τ becomes a larger component of total force production as *P. interruptus* increases in size. This increase in τ relative to total force production was predicted by Daniel and Meyhöfer (Daniel and Meyhöfer, 1989).

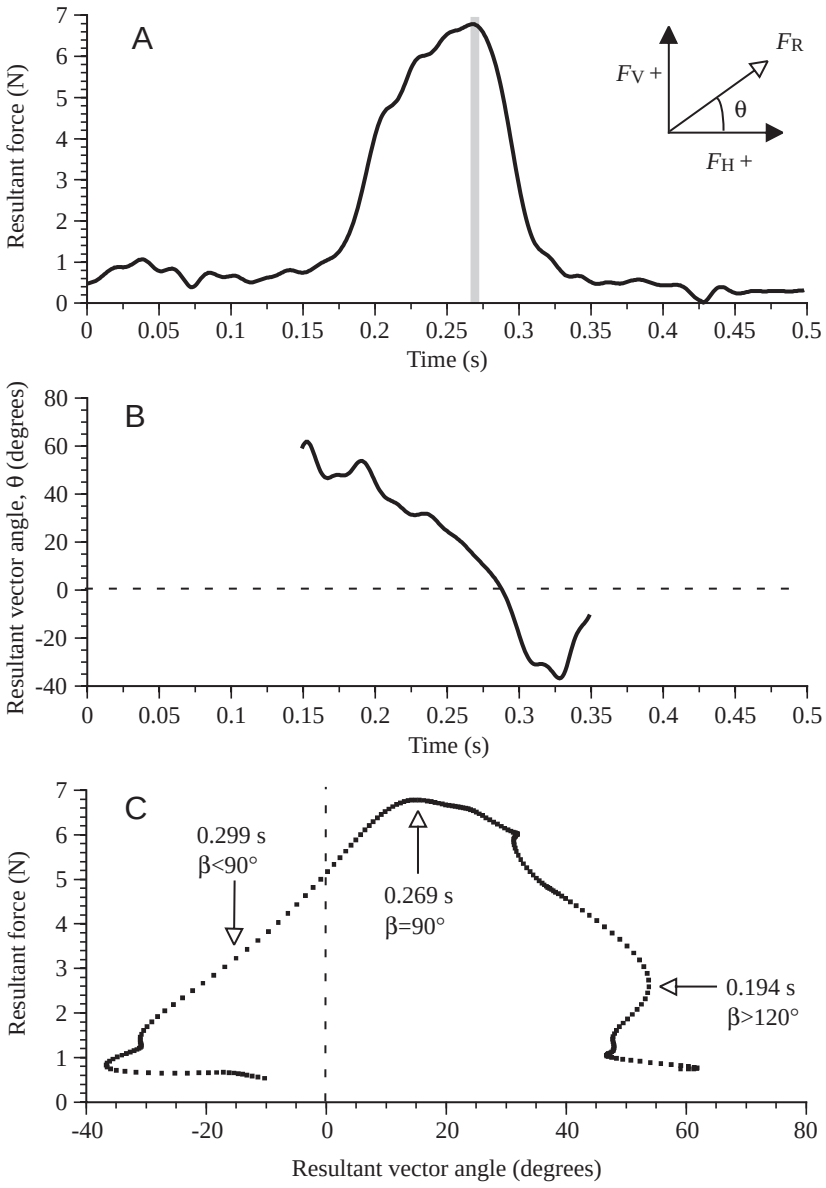


Fig. 6. The resultant force ($F_R$, A) and trajectory (θ, B) for the center of mass of a 165 g animal calculated from the horizontal $F_H$ and vertical $F_V$ forces shown in Fig. 5. At the time of maximum $F_R$, the tail was approximately normal to the body (the gray box in A is the time marker for the third video image in Fig. 5; the width of the box is the duration of a video image, 1/180 s. A polar plot (C) of $F_R$ (A) *versus* θ (B) shows that the vector angle of the resultant force was high (approximately 60 °) at the initiation of the flip and then decreased to approximately 20 ° at the time of maximum $F_R$ (the time points refer to Figs 5, 6A,B). Values of $F_{RMax}$ and θ at $F_{RMax}$ for all of the animals are presented in Table 1.

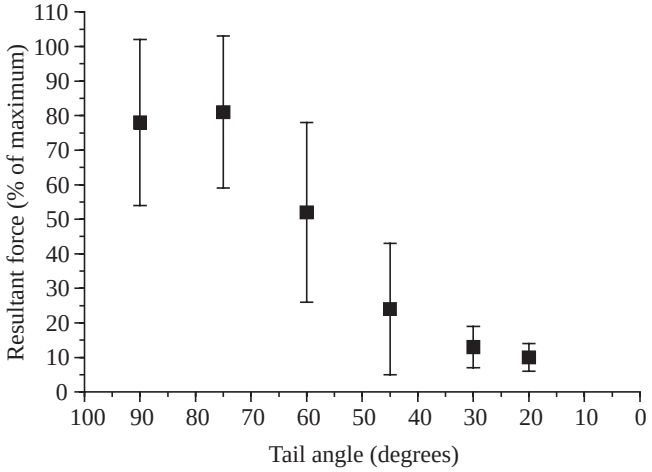


Fig. 7. The magnitude of the resultant force (percentage of maximum) as a function of the angle between the tail and the body (β). Values are means ± S.D. for five flips from each of the five animals (*N*=25). Note that β was approximately 15° when the tail was closed against the body because of the way the angle was defined (see Fig. 3 and Materials and methods).

*Methodological considerations*

There are several differences between the measurements made here and the forces produced by a free-swimming animal that initiates a flip while standing on a substratum. Our tethered animals were tail-flipping in mid-water (as detailed in the Materials and methods section). Spiny lobsters typically initiate tail-flips from the substratum (J. C. Nauen and R. E. Shadwick, personal observation) and then repeatedly tail-flip in mid-water. Flip events measured in mid-water do not involve any ground-reaction forces that might be produced by interactions between the legs, tail or moving fluid and the substratum. In addition, the animals were attached to the transducer and, thus, did not rotate or translate through the water during the flip. The lack of body rotation probably changed the trajectory angle of the thrust. The lack of translation may have affected hydrodynamic features of the starting and/or attached vortices forming at the tip of the tail. The forces associated with circulation of fluid around the translating body (Dickinson, 1996) would also have been disrupted by attachment to the transducer.

Ground-reaction forces and forces due to fluid circulation

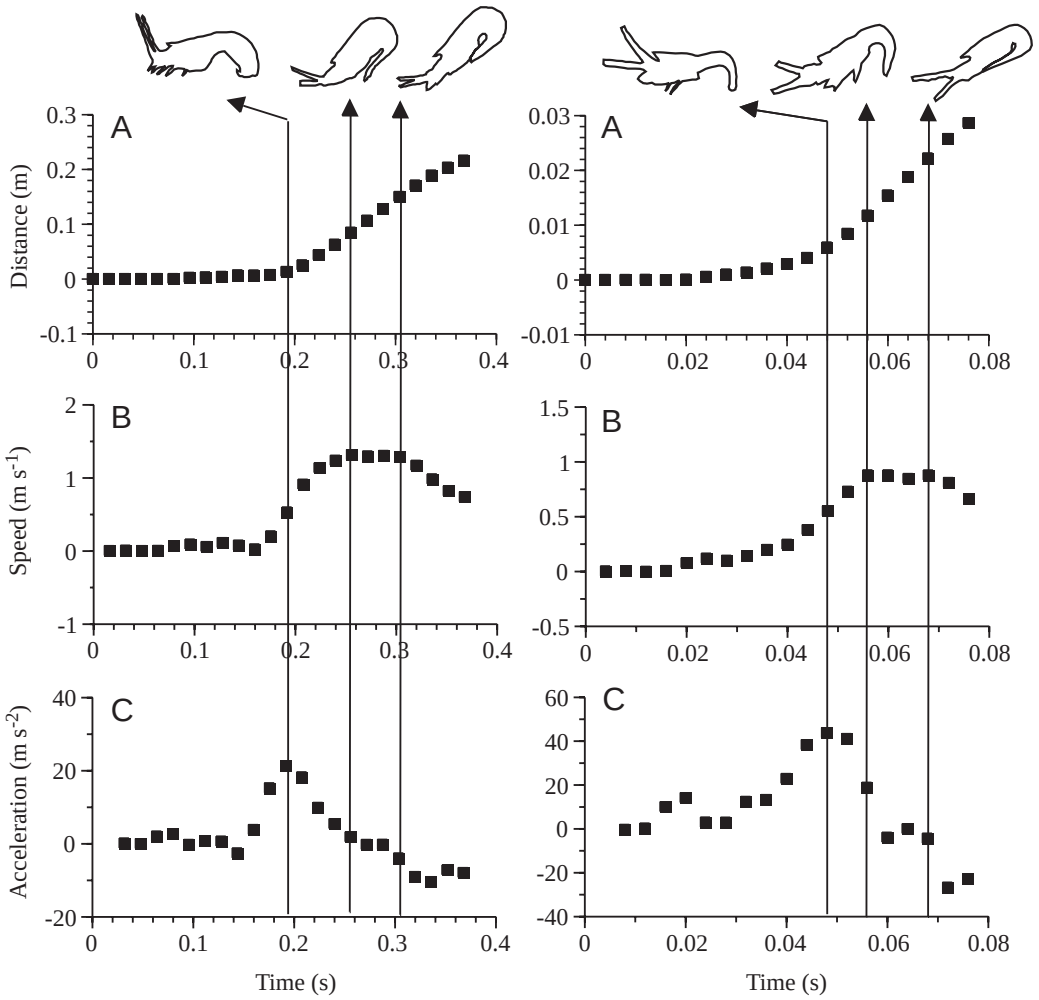


Fig. 8. The distance moved (A), speed (B) and acceleration of the body (C) of a free-swimming 1000 g body mass ($M_b$) animal (left) and a 1 g $M_b$ animal (right). Traced video images (not to scale) show the angle between the tail and the body (β) at the time points indicated.

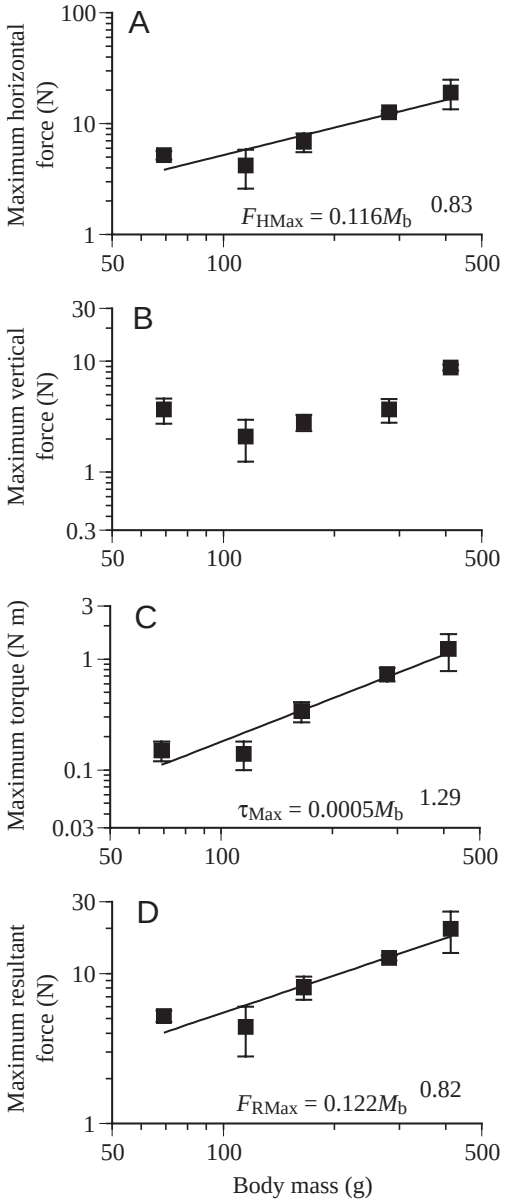


Fig. 9. Maximum horizontal force ($F_{HMax}$, A), maximum vertical force ($F_{VMax}$, B), maximum torque ($\tau_{Max}$, C) and maximum resultant force ($F_{RMax}$, D) as a function of body mass ($M_b$). Values are means ± S.D. ($N$=5). The lines represent the calculated power regression model of force on mass ($r^2$=0.85 for $F_{HMax}$, $r^2$=0.92 for $\tau_{Max}$, $r^2$=0.88 for $F_{RMax}$). Scaling statistics are presented in Table 5.

are secondary, however, to the thrust produced by the movement of the tail. In the model of Daniel and Meyhöfer (Daniel and Meyhöfer, 1989), movement of the tail created thrust as the sum of drag, added-mass and squeeze ($T_s$) forces as follows:

$$T(t) = \left[0.5\rho \int_0^L w C_{dl} du_n^2 dl + \rho \int_0^L \alpha_t A (du_n/dt) dl + T_s(t)\right] \sin\psi \,, \quad (4)$$

where $T$ is thrust, $t$ is time, ρ is the density of the fluid, $L$ is tail length, $w$ is tail width, $C_{dl}$ is the sectional drag coefficient of the tail, $u_n$ is the fluid velocity normal to the tail, $l$ is position along the tail, $\alpha_t$ is the sectional added-mass coefficient of the tail, $A$ is the local cross-sectional area of the tail, $T_s$ is the jet or squeeze force and ψ is the angle of the tail to the horizon (equation 5 of Daniel and Meyhöfer, 1989).

$T_s$ is calculated as:

$$T_s(t) = (2\rho/3) \int_0^L \frac{w^3}{h} \left[\frac{2}{h}\left(\frac{\partial h}{\partial t}\right)^2 - \frac{\partial^2 h}{\partial t^2}\right] dl \,, \quad (5)$$

where $t$ is time, ρ is the density of the fluid, $w$ is the local width of the tail, $l$ is position along the tail and $h$ is the local distance between the tail and the cephalothorax (equation 7 of Daniel and Meyhöfer, 1989). Thus, in this computational model, the forces contributing to thrust production in the tail-flip (drag, added-mass and squeeze forces) are directly dependent on the velocity and acceleration of the tail (Daniel and Meyhöfer, 1989).

Movement of the tail was unrestricted in the tethered animals, and a nested ANOVA analysis comparing the velocity and acceleration of the tail of tethered animals with that of a similar size range of free-swimming animals indicated no significant effect of tethering on tail kinematics. Thus, the present measurements made using the force transducer are representative of the performance of free-swimming animals and can be used to test hypotheses on the production of a jet force during tail-flipping and on the scaling of tail-flip force production.

### *The jet effect*

Force production from a jet formed when water is ejected as

Table 5. *Scaling characteristics of the force data for* Panulirus interruptus

| Figure number | Variable (units) | Variable range | $N$ | Predicted slope | OLS slope | OLS intercept | OLS $r^2$ | OLS S.E.M. of estimate | RMA slope, OLS slope/$r$ |
|---|---|---|---|---|---|---|---|---|---|
| 9A | $F_{HMax}$ (N) | 4.2–19.1 | 5 | 0.66 | 0.83±0.20* | 0.11±0.45 | 0.85 | 0.12 | 0.90* |
| 9C | $\tau_{Max}$ (N m) | 0.14–1.23 | 5 | 1.33 | 1.29±0.22* | 0.39±0.45 | 0.92 | 0.13 | 1.34* |
| 9D | $F_{RMax}$ (N) | 4.4–19.8 | 5 | 0.66 | 0.82±0.18* | 0.13±0.40 | 0.88 | 0.11 | 0.87* |

OLS, ordinary least-squares regression model; S.E.M., standard error of the mean; RMA, reduced major axis regression model; $F$, force; H, horizontal; Max, maximum; τ, torque; R, resultant.

*Slope is not significantly different from the predicted value.

OLS slope and intercept are given as means ± S.E.M.

two surfaces close against each other is an obvious locomotory mechanism for animals such as scallops (Cheng and DeMont, 1996). It has been proposed to play a less obvious, but important, role in force production for aquatic locomotory modes including pectoral-fin locomotion in fishes (Daniel and Meyhöfer, 1989; Geerlink, 1989) and swimming in the frog *Hymenochirus boettgeri* (Gal and Blake, 1988a; Gal and Blake, 1988b).

The existence of jet forces may be inferred if two body surfaces are in close proximity during the locomotory event and analysis of the motion in terms of forces such as drag, added-mass force and inertia do not account for the animal's performance. For example, in one study of frog swimming (Gal and Blake, 1988a), force production was modeled using drag and inertial terms based on measurements of hind-limb kinematics. As values of drag and inertia failed to account for the observed acceleration of the body during the latter half of the stroke, when the feet are in close proximity, it was inferred (Gal and Blake, 1988a) that interaction effects between the limbs (jet or reflective effects) might be important for force production during the latter half of the stroke. Alternatively, computational models of swimming mechanics (such as that of Daniel and Meyhöfer, 1989), which include a jet component and accurately predict locomotory kinematics, also infer the production of a jet.

Jet forces produced as two body surfaces close against each other during locomotion have only been observed or measured, however, for confirmed jet locomotors such as scallops. For example, Geerlink (Geerlink, 1983) hypothesized that, as the pectoral fin of a fish closed against the body, a downstream-directed jet formed that contributed to thrust production. Drucker and Lauder (Drucker and Lauder, 1999) did not see such a jet in their flow visualization study of pectoral fin locomotion by the bluegill sunfish *Lepomis macrochirus*, so they concluded that thrust produced by vortex ring shedding from the pectoral fins is not substantially augmented by squeeze or jet force production.

The present concurrent measurements of force production and kinematics during the tail-flip escape response do not support the hypothesis that a strong jet is produced as the tail closes against the body. Intuitively, one would expect a jet to form in the latter half of the flip as the tail closes against the body, and in the computational model (Daniel and Meyhöfer, 1989), jet forces rise to maximal values as β decreases from approximately 40 to 15 ° (estimated from their Figs 7 and 8). On the basis of Fig. 8 in Daniel and Meyhöfer (1989), maximal forces of approximately 2.0 N (determined by summing the values of *x*-component and *y*-component forces at the 15 ms peak) occurred mid-flip and then declined. A second peak in force production in the last 5 ms (or 17 %) of the flip reached maximum values of approximately 1.3 N, or approximately 65 % of the maximum force for the flip; jet forces were approximately 70 % of this secondary peak. Thus, the model predicts a second force peak of appreciable size as the tail closes against the body and a strong contribution of jet forces to that second force peak.

The present data indicate that the forces produced during the last third of the flip by *Panulirus interruptus* fall to approximately 15 % of maximum values, which is less than a quarter of what is predicted by the Daniel and Meyhöfer model (Daniel and Meyhöfer, 1989). Given that drag and added-mass forces are still produced at this time because the tail has some velocity and is decelerating, jet force levels are necessarily less than 25 % of what is predicted by the mathematical model (Daniel and Meyhöfer, 1989). Thus, the present data indicate that *P. interruptus* is not producing a high-force jet of water as the tail closes against the body at the end of a tail-flip.

Six morphological variables were factors in the Daniel and Meyhöfer model (Daniel and Meyhöfer, 1989), so differences in shape between the shrimp *Pandalus danae* and the lobster *Panulirus interruptus* examined here could contribute to the disparity in results. The shape of the tail is very important in calculations of thrust production by the model. For example, tail length is a factor in each of the three forces (drag, added-mass and squeeze force) contributing to thrust production. In addition, drag is dependent on the width of the tail ($w$), added-mass forces are dependent on $w^2$ and squeeze forces are dependent on $w^3$ (Daniel and Meyhöfer, 1989). Thus, tail shape is a factor in each of the three forces contributing to thrust and is most important for the jet force. However, the tail of *Panulirus interruptus* is relatively wider and longer than that of *Pandalus danae* (Nauen and Shadwick, 1999), giving the lobster a morphological advantage over the shrimp for producing thrust, and especially a jet force. Body shape is independent of size for both species because of isometric growth, so the absence of a jet force in *Panulirus interruptus* is not attributable to an obvious difference in body shape between the lobster and the shrimp.

The difference in size between the individuals of *Pandalus danae* examined by Daniel and Meyhöfer (2–8 g $M_b$) and the individuals of *Panulirus interruptus* examined here (69–412 g $M_b$) is another possible factor in the disparity in results between the two studies. The mass of the lobsters tested in the present study was limited to a range of approximately 70–400 g $M_b$ because of the resonant frequency of the force transducer. Force measurements from animals in this size range indicated that, on average, maximum force is produced when the tail is approximately normal to the body (and β values were 75–90 °). Kinematic data for free-swimming individuals of *Panulirus interruptus* ranging from 1 to 1000 g $M_b$ (spanning the size range of the shrimp) indicated that, irrespective of body size, maximum acceleration of the $C_m$ occurred when the tail was positioned approximately normal to the body, and deceleration of free-swimming animals, concurrent with maximum velocity, occurred when β was approximately 35 °. Thus, kinematic measurements of free-swimming animals ranging in $M_b$ over three orders of magnitude do not indicate substantial production of force as the tail closes against the body and β decreases from approximately 45 to 15 °. The size-independence of the kinematic data suggests that the low force production seen as the tail closed against the body in the

present study is probably not attributable to the size of the lobsters examined.

If it is the case that the shrimp *Pandalus danae* produces a strong jet during the tail-flip, as predicted by the Daniel and Meyhöfer model (Daniel and Meyhöfer, 1989), differences in three performance factors might contribute to the discrepancy between the model output and the present results. Tail-flip durations for *Panulirus interruptus* of any size are longer than those for *Pandalus danae* and, although both species move a similar distance relative to their body length *BL* (approximately 0.7*BL*), calculated maximum velocities and accelerations for *Pandalus danae* are up to twice those for *Panulirus interruptus* (see Table 3 in Nauen and Shadwick, 1999). These differences in performance are probably related to the large abdominal muscle mass of *Pandalus danae* (approximately 40 % of $M_b$; Meyhöfer and Daniel, 1990) compared with *Panulirus interruptus* (approximately 22 % of $M_b$; Nauen and Shadwick, 1999). Although the tail of *Panulirus interruptus* reaches high maximum accelerations (of the order of $100\,m\,s^{-2}$ for free-swimming animals as large as 100 g $M_b$; Nauen and Shadwick, 1999, which is within the size range of animals tested on the transducer in the present study), it is possible that these accelerations are too low to create the high squeeze force predicted by the model. Empirical studies of force production by *Pandalus danae* using flow visualization or force measurement techniques, or modeling the flip of *Panulirus interruptus*, would address the questions raised by the differences in the dynamics of tail-flip force production indicated by these two studies.

The present force and kinematic data indicate that the tail of *Panulirus interruptus* acts largely as a paddle and that the forces produced during tail-flipping are predominantly added-mass forces and drag. Crustaceans lack the defined internal cavity and/or aperture for forming a directed jet that characterizes confirmed jet locomotors, and it seems likely that during the tail-flip water is forced out laterally as well as anteriorly as the tail closes. Testing this theory requires new experiments in which any lateral forces produced during the flip are also measured or the flow around the tail is visualized by the addition of a marker to the fluid.

While complete adduction of the tail to the cephalothorax may not contribute substantially to force production, it does result in a streamlined shape for the animal that bears a strong resemblance to an airfoil at a low angle of attack. Lobsters often glide for distances equal to several body lengths between tail-flips. Full flexion of the tail undoubtedly increases their gliding distance by reducing drag and possibly by enhancing fluid circulation around the body. If the animal tail-flips several times in rapid succession, complete adduction of the tail to the body would allow the animal to extend the tail in a relatively low-profile manner that would limit disruption of the glide.

### *The scaling of force production*

It was predicted that muscle force would scale as abdominal cross-sectional area, or $M_b^{2/3}$, because of isometric growth (McMahon, 1984; Daniel and Meyhöfer, 1989). $F_{HMax}$ increased as $M_b^{0.83}$ or $M_b^{0.90}$ (OLR and RMA models, respectively). $F_{RMax}$ increased as $M_b^{0.82}$ or $M_b^{0.87}$ (OLR and RMA models, respectively). These slopes suggest that, relative to body size, force production increases at a rate greater than would be predicted from increases in abdominal muscle cross-sectional area (although none of the slopes is statistically different from the isometric value of 2/3 because of the relatively large standard errors of the slope estimate and the small $N$ value). Kinematic data indicate that the speed and acceleration of the tail are independent of body size for both free-swimming (Nauen and Shadwick, 1999) and tethered animals, and that the acceleration of the $C_m$ of free-swimming animals is size-independent (Nauen and Shadwick, 1999). Taken together, these data suggest that maximum stress limits of the abdominal muscle of *Panulirus interruptus* scale with a mass exponent greater than 2/3.

An increase in muscle force output could be the result of increased muscle cross-sectional area, as in the case of the ungulate plantaris muscle (Pollock and Shadwick, 1994). This is unlikely to be happening in *Panulirus interruptus*, however, because the abdomen shows isometric increases in length and width and is packed with muscle at all sizes, so an increase in muscle cross-sectional area would depend on a decrease in muscle fiber length. The abdominal muscle of *Panulirus interruptus* is a repeating series of six muscles in a complex helical arrangement (for a detailed description of palinurid muscle, see Daniel, 1931). This morphology, which is presumed to increase the speed and power of tail contraction, was considered by Rayner and Wiersma (Rayner and Wiersma, 1963; Rayner and Wiersma, 1967). Changes in the geometry of the muscle arrangement with increases in body size could contribute to a relative increase in muscle force output. Alternatively, muscle fiber characteristics such as white muscle enzyme activity (which scales positively in pelagic fish; Somero and Childress, 1990) or myosin composition (as examined in the short-horned sculpin *Myoxocephalus scorpius*; James et al., 1998) may occur in lobster abdominal muscle. It is known that the developmental dynamics of some crustacean muscle includes continuous fiber growth and fiber type transformation (Mellon, 1992), but the scaling of the contractile characteristics of lobster abdominal muscle remains unexplored.

The scaling of torque as $M_b^{1.29}$ or $M_b^{1.34}$ (for the OLR and the RMA models, respectively) indicates that with increased $M_b$ torque becomes a relatively larger component of the total force produced during the tail-flip. These slopes were not significantly different from the hypothesized scaling relationship of $M_b^{4/3}$. The kinematics of free-swimming animals can be predicted from these data. The rotational analog for force = mass × acceleration is $\tau=I\alpha$, where $I$ is the moment of inertia and $\alpha$ is the angular acceleration. The moment of inertia for a beam rotating about its center is $I=mr^2/12$, where $m$ is beam mass and $r$ is beam length. Given geometric similarity, $r\propto m^{1/3}$ and $I\propto m^{5/3}$. Thus, $\tau\propto m^{4/3}$ and $\alpha\propto m^{-1/3}$. Applying this logic to the tail-flip results in the hypothesis that rotational acceleration of the body will decrease as $M_b^{-0.33}$.

Measurements of free-swimming animals weighing from 1 to 1000 g $M_b$ indicated that $\alpha \propto M_b^{-0.28}$, with a standard error of the slope of 0.084. The scaling relationship of $\alpha$ based on kinematic measurements was not significantly different from the predicted value (Nauen and Shadwick, 1999). The present measurements indicted that $\tau \propto M_b^{1.29}$ with a standard error of the slope of 0.22. Using this value, one would predict $\alpha$ to scale as $M_b^{-0.38}$, which was also not significantly different from the predicted value ($P$>0.5). Thus, both force measurements on tethered animals and kinematic data from free-swimming animals support scaling predictions for $\tau$ and $\alpha$ that are based on simple geometric theory.

The use of the transducer treats the animal as a 'black box' and provides an overall measurement of how force output scales with body size. The results of the force measurements presented here and of previous kinematic experiments (Nauen and Shadwick, 1999) suggest that the abdominal flexor musculature may show interesting changes in its contractile characteristics as body size increases. These two lines of evidence support further, more detailed studies of the contractile kinetics and muscle geometry. More detailed studies of the functional morphology of the flexor muscle (such as the study of the extensor muscles; Meyhöfer and Daniel, 1990) would begin to bridge the gap between the studies with a biomechanical basis and the vast literature on the neurophysiology of this behavior (e.g. Wine and Krasne, 1984; Edwards et al., 1994a; Edwards et al., 1994b) and would provide an interesting case study of muscles used for acceleratory locomotion.

We thank Dr Steve Katz for his long-standing assistance with this project and Dr John Gosline for his extremely helpful suggestions for designing and building the force transducer. We thank Dr G. Lauder for his assistance with statistical analyses. This paper was greatly improved by suggestions from two anonymous reviewers and by Drs P. Franks, T. Knower, M. Latz, A. McCulloch, J. Rohr, R. Rosenblatt, G. Szulgit, E. Freund and P. Johnston. R. McConnaughey collected and helped to maintain the animals used in this study. J.C.N. was supported by scholarship grants from Scripps Institution of Oceanography, Achievement Rewards for College Scientists, International Women's Fishing Association and Woman's Farm and Garden Association. R.E.S was supported by NSF IBN95-14203.

## References

**Arnott, S. A., Neil, D. M. and Ansell, A. D.** (1998). Tail-flip mechanism and size-dependent kinematics of escape swimming in the brown shrimp *Crangon crangon*. *J. Exp. Biol.* **201**, 1771–1784.

**Biewener, A. A. and Full, R. J.** (1992). Force platform and kinematic analysis. In *Biomechanics (Structures and Systems): A Practical Approach* (ed. A. A. Biewener), pp. 45–73. Oxford: Oxford University Press.

**Cheng, J. Y. and DeMont, M. E.** (1996). Jet-propelled swimming in scallops: Swimming mechanics and ontogenetic scaling. *Can. J. Zool.* **74**, 1734–1738.

**Cromarty, S. I., Cobb, J. S. and Kass-Simon, G.** (1991). Behavioral analysis of the escape response in the juvenile lobster *Homarus americanus* over the molt cycle. *J. Exp. Biol.* **158**, 565–581.

**Daniel, R. J.** (1931). The abdominal muscular systems of *Homarus vulgaris* (L.) and *Palinurus vulgaris* (Latr.). *Proc. Trans. Liverpool Biol. Soc.* **45**, 3–71.

**Daniel, T. L. and Meyhöfer, E.** (1989). Size limits in escape locomotion of carridean shrimp. *J. Exp. Biol.* **143**, 245–265.

**Dickinson, M. H.** (1996). Unsteady mechanisms of force generation in aquatic and aerial locomotion. *Am. Zool.* **36**, 537–554.

**Domenici, P. and Blake, R. W.** (1993). The effect of size on the kinematics and performance of angelfish (*Pterophyllum eimekei*). *Can. J. Zool.* **71**, 2319–2326.

**Drucker, E. G. and Lauder, G. V.** (1999). Locomotor forces on a swimming fish: three-dimensional vortex wake dynamics quantified with digital particle image velocimetry. *J. Exp. Biol.* **202**, 2393–2412.

**Edwards, D. H., Fricke, R. A., Barnett, L. D., Yeh, S.-R. and Leise, E. M.** (1994a). The onset of response habituation during growth of the lateral giant neuron of crayfish. *J. Neurophysiol.* **72**, 890–898.

**Edwards, D. H., Yeh, S.-R., Barnett, L. D. and Nagappan, P. R.** (1994b). Changes in synaptic integration during the growth of the lateral giant neuron of crayfish. *J. Neurophysiol.* **72**, 899–908.

**Full, R. J. and Tu, M. S.** (1990). Mechanics of six-legged runners. *J. Exp. Biol.* **148**, 129–146.

**Gal, J. M. and Blake, R. W.** (1988a). Biomechanics of frog swimming. I. Estimation of the propulsive force generated by *Hymenochirus boettgeri*. *J. Exp. Biol.* **138**, 399–411.

**Gal, J. M. and Blake, R. W.** (1988b). Biomechanics of frog swimming. II. Mechanics of the limb-beat cycle in *Hymenochirus boettgeri*. *J. Exp. Biol.* **138**, 413–429.

**Geerlink, P. J.** (1983). Pectoral fin kinematics of *Coris formosa* (Teleostei, Labridae). *Neth. J. Zool.* **33**, 515–531.

**Geerlink, P. J.** (1989). Pectoral fin morphology: A simple relation with movement pattern? *Neth. J. Zool.* **39**, 166–193.

**Heitler, W. J., Fraser, K. and Ferrero, E. A.** (2000). Escape behavior in the stomatopod crustacean *Squilla mantis* and the evolution of the caridoid escape reaction. *J. Exp. Biol.* **203**, 183–192.

**Huxley, J. S.** (1932). *Problems of Relative Growth*. New York: The Dial Press.

**James, R. S., Cole, N. J., Davies, M. L. F. and Johnston, I. A.** (1998). Scaling of intrinsic contractile properties and myofibrillar protein composition of fast muscle in the fish *Myoxocephalus scorpius* L. *J. Exp. Biol.* **201**, 901–912.

**LaBarbera, M.** (1989). Analyzing body size as a factor in ecology and evolution. *Annu. Rev. Ecol. Syst.* **20**, 97–117.

**McMahon, T. A.** (1984). *Muscles, Reflexes and Locomotion*. Princeton, NJ: Princeton University Press.

**Mellon, D.** (1992). Connective tissue and supporting structures. In *Microscopic Anatomy of Invertebrates*, vol. 10 (ed. F. W. Harrison and A. G. Humes), pp. 77–116. New York: Wiley-Liss.

**Meyhöfer, E. and Daniel, T.** (1990). Dynamic mechanical properties of the extensor muscle cells of the shrimp *Pandalus danae*: cell design for escape locomotion. *J. Exp. Biol.* **151**, 435–452.

**Milnor, W. R.** (1982). *Hemodynamics*. Baltimore: Williams & Wilkins.

**Nauen, J. C. and Shadwick, R. E.** (1999). The scaling of acceleratory aquatic performance: body size and tail-flip performance of the California spiny lobster *Panulirus interruptus*. *J. Exp. Biol.* **202**, 3181–3193.

**Newland, P. L., Chapman, C. J. and Neil, D. M.** (1988). Swimming performance and endurance of the Norway lobster *Nephrops norvegicus*. *Mar. Biol.* **98**, 345–350.

**Newland, P. L., Neil, D. M. and Chapman, C. J.** (1992). Escape swimming in the Norway lobster. *J. Crust. Biol.* **12**, 342–353.

**Pollock, C. M. and Shadwick, R. E.** (1994). Allometry of muscle, tendon and elastic energy storage capacity in mammals. *Am. Physiol. Soc.* **266**, 1022–1031.

**Rayner, M. D. and Wiersma, C. A. G.** (1963). Functional aspects of the anatomy of the main thoracic and abdominal flexor musculature of the crayfish *Procambarus clarkii* (Girard). *Am. Zool.* **4**, 285.

**Rayner, M. D. and Wiersma, C. A. G.** (1967). Mechanisms of the crayfish tail flick. *Nature* **213**, 1231–1232.

**Sokal, R. R. and Rohlf, F. J.** (1995). *Biometry*. Third edition. New York: W. H. Freeman & Company.

**Somero, G. N. and Childress, J. J.** (1990). Scaling of ATP-supplying enzymes, myofibrillar proteins and buffering capacity in fish muscle: relationship to locomotory habitat. *J. Exp. Biol.* **149**, 319–333.

**Spanier, E., Weihs, D. and Almog-Shtayer, G.** (1991). Swimming of the Mediterranean slipper lobster. *J. Exp. Mar. Biol. Ecol.* **145**, 15–31.

**Tegner, M. J. and Levin, L. A.** (1983). Spiny lobsters and sea urchins: analysis of a predator–prey interaction. *J. Exp. Mar. Biol. Ecol.* **73**, 125–150.

**Webb, P. W.** (1976). The effect of size on the fast-start performance of rainbow trout *Salmo gairdneri* and a consideration of piscivorous predator–prey interactions. *J. Exp. Biol.* **65**, 157–177.

**Webb, P. W.** (1979). Mechanics of escape responses in crayfish (*Orconectes virilis*). *J. Exp. Biol.* **79**, 245–263.

**Wine, J. J.** (1984). The structural basis of an innate behavior pattern. *J. Exp. Biol.* **112**, 283–319.

**Wine, J. J. and Krasne, F. B.** (1984). The cellular organization of crayfish escape behavior. In *The Biology of Crustacea*, vol. 4 (ed. D. C. Sandeman and H. L. Atwood), pp. 241–292. New York: Academic Press.

**Winter, D. A.** (1989). *Biomechanics and Motor Control of Human Movement*. New York: John Wiley & Sons, Inc.

**Zar, J. H.** (1984). *Biostatistical Analysis*. Second edition. Englewood Cliffs, NJ: Prentice Hall.